2D Materials

PAPER • OPEN ACCESS

Covalent cross-linked graphene oxide aerogels for moisture adsorption

To cite this article: Zhijian Cao *et al* 2025 *2D Mater.* **12** 045010

IOP Publishing 2D Mater. 12 (2025) 045010 https://doi.org/10.1088/2053-1583/ae01ba

2D Materials

OPEN ACCESS

RECEIVED
30 April 2025

REVISED
1 August 2025

ACCEPTED FOR PUBLICATION
2 September 2025

PUBLISHED
11 September 2025

PAPER

Covalent cross-linked graphene oxide aerogels for moisture adsorption

Zhijian Cao[1], **Xiaojun Ren**[1], **Tongxi Lin**[1,*], **Yuta Nishina**[2], **Masamichi Yoshimura**[3] and **Rakesh Joshi**[1,*]

[1] School of Materials Science and Engineering, University of New South Wales, Sydney NSW, 2052, Australia
[2] Research Institute for Interdisciplinary Science, Okayama University Kita-ku, Okayama 700-8530, Japan
[3] Graduate School of Engineering, Toyota Technological Institute, Nagoya 468–8511, Japan
[*] Authors to whom any correspondence should be addressed.

E-mail: tongxi.lin@student.unsw.edu.au and r.joshi@unsw.edu.au

Keywords: graphene oxide (GO), covalent cross-linking, poly(ethylene glycol) (PEG), moisture adsorption, hydrophilicity enhancement

Abstract

Covalent cross-linking is an effective approach to enhance the hydrophilicity and water adsorption properties of graphene oxide (GO). We studied moisture absorption in GO cross-linked with poly(ethylene glycol) diamines. At relative humidity (RH) of 85%, the PEG-cross-linked GO exhibited a significantly enhanced water uptake capacity of 0.59 g of water per gram of GO (gg^{-1}), compared to 0.37 for unmodified GO. This is attributed to the presence of alkoxy groups via cross-linking, resulting in the enhanced interaction between GO and water molecules. These findings highlight the potential of PEG-based covalent functionalisation for efficient moisture capture in GO-based materials.

1. Introduction

Traditional solid porous adsorbents such as silica gels and zeolites are widely used as the desiccant materials for water adsorption from the atmosphere [1, 2]. However, the limited surface area, high energy consumption, and low hydrophilicity of these materials offer constrained water adsorption efficiency. Porous adsorbent material in desiccant applications, such as metal-organic frameworks have shown high performance in adsorption capacity. However, the low commercial feasibility still highly limits the scalability [3, 4]. Chemical adsorbents such as hygroscopic salts have also exhibited great adsorption capacity; however, significant challenges such as deliquescence, corrosion, and low cycling stability are still difficult to overcome [5]. As a two-dimensional (2D) material, many studies have explored the interaction between graphene oxide (GO) and water molecules [6–12]. The abundant oxygen-containing functional groups on GO act as active dipole sites [13–17], forming an interfacial hydrogen bond network [18–21] which significantly affects the diffusion rate of water molecules [22, 23]. Moreover, the large surface area, inherent porous networks, and tunable interlayer spacing [24, 25] make GO a promising candidate as a solid adsorbent for desiccant applications [26, 27]. Previous studies have shown multiple modification approaches on GO-based materials for enhanced atmospheric water capture applications. For instance, Wang *et al* [28] used $CaCl_2$ to fabricate calcium chloride ($CaCl_2$)/GO/poly(N-isopropylacrylamide) gel, exhibiting adsorption capacity of 3.6 gg^{-1}. Anjali *et al*[29] added lithium chloride (LiCl) into GO/poly(vinyl alcohol) (GO/PVA) mixed hydrogel to fabricate a hygroscopic salt-embedded gel, which performed water uptake of 1.2 gg^{-1}. The authors demonstrated that LiCl mainly adsorbs water vapour, and PVA retains the collected water in the gel [29]. There is still a knowledge gap in using salt-free covalently cross-linked GO-based materials for moisture adsorption. Among the abundant GO-based covalent cross-linking strategies, polyethylene glycol-diamine (PEGDA) is widely used as a hydrophilic cross-linking reagent to bring new functions to GO via covalent interactions, such as esterification and amidation [30]. Amidation is known as the extensively used covalent cross-linking strategy for PEG-GO functionalisation. This method typically requires the utilisation of coupling agents such as 1-ethyl-3-(3-dimethylaminopropyl) carbodiimide hydrochloride and N-Hydroxysuccinimide [31–33]. However, for moisture adsorption applications, most of the effective covalent cross-linking methods face challenges such as high energy consumption, large financial costs, and toxicity. Interestingly, catalysts are not necessary in the reaction between GO and amine groups via epoxy ring openings due to the high reactivity of epoxides towards amine derivatives [34]. Hence, the innovation of PEG-GO fabricated through the epoxy ring opening reaction is highly promising for studying the role of covalent cross-linking in moisture adsorption applications, which have been employed to various biomedical applications as reported [35–38]. Zhao *et al* [39] fabricated novel sodium alginate /PEGDA-GO composite membranes via the covalent cross-linking between epoxy groups on GO and the amino groups on PEGDA. The authors demonstrated that the composite membranes exhibited significantly improved hydrophilicity due to the abundant ether bonds sourced from PEGDA, and a brand-new C–N covalent bond effectively controlled the interlayer d-spacing of GO [39]. Inspired by this and our previous works [40, 41], we used PEGDA as the source of amino groups to synthesise cross-linked PEG-GO aerogel PEG-GOA. This work studies the effects of covalent cross-linking on GO-based moisture adsorption, and the mechanisms behind the synergistic effects of polymer-GO nanocomposites for enhanced water adsorption applications.

2. Experimental methods

2.1. Materials

GO suspension (1.5 wt% suspension with a flake size of 0.5 μm was supplied by NiSiNa Materials Japan. Calcium chloride ($CaCl_2$), magnesium chloride ($MgCl_2$), magnesium nitrate ($Mg(NO_3)_2$), sodium chloride (NaCl), potassium chloride (KCl), and copper chloride ($CuCl_2$) salt powders were purchased from Sigma-Aldrich for making saturated salt solutions. The cross-linking reagent PEGDA ($Mw = 3{,}000\ g\ mol^{-1}$) was also obtained from Sigma-Aldrich.

2.2. Fabrication of cross-linked PEG-GOA

The cross-linked PEG-GO solution was prepared by adding a predetermined mass of PEGDA powder to the GO suspension. In detail, PEGDA powder was weighed and added to the GO suspension in increasing amounts from 5 to 30 mg, which corresponded to 5% – 30% of mass fraction relative to the mass of GO (100 mg). After the 1 h continuous magnetic stirring, the obtained PEG-GO mixture was freeze-dried to form the aerogel samples. The samples were tightly sealed to control the moisture.

2.3. Characterisation

The Fourier transform infrared (FTIR) spectroscopy (PerkinElmer Spectrum Two), x-ray photoelectron spectroscopy (XPS), and liquid-state ^1H nuclear magnetic resonance (NMR) were used to characterise the chemical bonds and examine the immobilisation of PEG on GO. For XPS, we used the Shirley method in Origin software to subtract the baseline, and Gaussian was performed for the peak fitting using 284.5 eV as the reference for the C1s peak of graphite. Scanning electron microscope (SEM) was used to investigate the surface morphologies of aerogel samples. In this study, SEM images were obtained from NanoSEM 450 field-emission scanning electron microscope (FE-SEM). X-ray diffraction (XRD) (PANalytical Empyrean I-Cu powder) was used to measure the interlayer spacings of aerogel samples with Cu K-alpha radiation at 45 kV and 40 mA based on $\lambda = 0.1541$ nm. The d-spacing is calculated based on Bragg's law, which is consistent with many previous studies [42–44]. Moreover, transmission electron microscope (TEM) with energy dispersive spectra (EDS) was conducted to further study the morphology of PEG-GO flake and investigate the elemental distributions on the flake.

Table 1. Summary of partial pressures controlled by different saturated salt solutions.

Saturated salt solution	Relative humidity	Partial pressures
$MgCl_2$	35%	1.11 kPa
$Mg(NO_3)_2$	55%	1.74 kPa
$CuCl_2$	65%	2.06 kPa
NaCl	75%	2.38 kPa
KCl	85%	2.69 kPa

2.4. Measurements of water uptake

We used a highly sensitive electronic mass balance in a controlled environment to measure the mass changes to calculate the amount of adsorbed water. The initial mass of the freeze-dried aerogel sample (m_i) was measured, and saturated salt solutions were used to control the different relative humidity (RH). Afterward, the aerogel sample was placed in a cleaned petri dish, and the total mass before and after the adsorption/desorption processes (m_{f1} and m_{f2}) was measured to calculate the water uptake.

We calculated partial pressures based on the controlled RH using equation (1):

$$\varphi = \left(\frac{p_w}{p_{ws}}\right) * 100\% \qquad (1)$$

where φ is the RH (%), p_w and p_{ws} represent the vapour partial pressure (kPa) and saturated vapour partial pressure (kPa). In this study, we used 3.17 kPa as the p_{ws} value under ambient temperature (25 °C). Table 1 below shows the calculated partial pressures corresponding to the RH controlled by saturated salt solutions [45, 46]. Particularly for the RH of 20%, we used calcium chloride ($CaCl_2$) powder to control.

Table 1 below shows the calculated partial pressures corresponding to the RH controlled by saturated salt solutions. Particularly for the RH of 20%, we used calcium chloride ($CaCl_2$) powder to control.

3. Results and discussion

To study the covalent reaction between PEGDA and GO, as schematically illustrated in figure 1(a), the aerogel samples were first characterised by FTIR spectroscopy. As shown in figure 1(b), the bands at 3143, 1721, and 1629 cm^{-1} are attributed to hydroxyl (–OH), carboxyl (C=O), and aromatic C=C stretching [47, 48]. The peak at 1400 cm^{-1} belongs to the bending vibration of hydroxyl (–OH) [49], and the two bands at 1105 and 1067 cm^{-1} were due to the stretching vibrations of epoxy (C–O–C) and alkoxy (C–O) [50–52]. After cross-linking, three bands from PEGDA powder can be clearly observed at 2870, 1349, and 1248 cm^{-1} on PEG-GOA, which are related to the stretching band of C–H [50, 53, 54], $–CH_2$ groups [55], and the C–N stretching vibration band [55–57]. Moreover, for the spectra of PEG-GOA (10%) and PEG-GOA (30%), as the amount of PEGDA increases, a gradual increase in the absorption intensity at 1076 cm^{-1} can be observed. This indicates the introduction of more alkoxy groups because of the cross-linking [39]. Most importantly, PEG-GOA (10%) and PEG-GOA (30%) also reveal a rising intensity of the C–N vibration band at 1248 cm^{-1}, strongly suggesting the successful cross-linking between PEGDA and GO [39]. Figures 1(c) and (d) display the XPS high-resolution C1s spectra of PEG-GOA and pure GOA samples, where three characteristic peaks can be observed at binding energies of 284.5, 286.6, and 288.3 eV for pure GO, corresponding to C–C/C=C, C-O-C/C–O, and C=O, respectively [58–61]. For the PEGDA modified PEG-GOA in figure 1(d), a distinct peak appears at the binding energy of 285.8 eV, corresponding to the C–N bond [39]. This indicates the reaction between amino groups on PEGDA and epoxy groups on GO, suggesting that the cross-linking is covalent. After the cross-linking, the introduction of more hydrophilic functional groups supports the increase in water adsorption ability of PEG-GOA.

Notably, figure 1(c) shows one peak at 291.3 eV, which was possibly associated with the shake-up feature of aromatic structures or π–π^* transition [62], and another peak at about 289.6 eV. These two peaks are not aligned with the characteristic peaks of GO before or after the cross-linking; hence, we cannot understand the origin of these peaks. The above information demonstrates the epoxy ring opening reaction [39, 63], further indicating that the cross-linking between PEGDA and GO was covalent.

Liquid-state ^{1}H NMR was conducted in this study to examine the successful immobilisation of PEG on GO after the cross-linking. In figure 2, the characteristic peak of PEG, which is located at ~3.62 ppm [64, 65], is negligible in the spectrum of PEG-GO. Hence, the PEG is immobilised on GO within the cross-linked PEG-GO composite.

We used XRD to observe the changes in the interlayer structure after cross-linking. Figure 2(b) displays the XRD patterns of pure GO and PEG-GOA samples in the dry state, which highlights that the introduction of a 10% mass fraction of PEGDA enhanced the interlayer spacing of GO laminates from 8.9 Å to 9.3 Å. Subsequently, the interlayer spacing of PEG-GOA (30%) was significantly increased from 9.3 Å to 11.0 Å. Therefore, the gradually increased interlayer spacings in the dry state demonstrate the presence of grafted PEG polymers in the interlayer region of PEG-GOA after covalent cross-linking. Furthermore, because of the nature of 2D materials, this observed continuous improvement in the interlayer spacings after cross-linking also indicates the developments in the porosity of GO [26, 40, 66, 67]. In figure 2(b), the interlayer spacing of wet pure GOA increased by only 0.2 Å, while the d-spacing of PEG-GOA (10%) considerably increased from 9.3 Å to 10.5 Å. However, when the mass fraction of PEGDA further increases to 30%, the d-spacing in the wet state is slightly increased by 0.7 Å. This suggests that the increased amount of grafted PEGDA polymers in the interlayer space of PEG-GOA limited the swelling.

Additionally, we conducted scanning electron microscopy (SEM) to study the surface morphology of cross-linked PEG-GOA. The surface morphologies of pure GOA and the PEG-GOA prepared with mass fractions of 10% and 30% are displayed in figures 3(a)–(f). The SEM images show that GOA exhibited a porous structure before and after the cross-linking. Additionally, compared to the relatively smooth surface exhibited by pure GOA in figure 3(d), the appearance of larger aggregated wrinkles on the PEG-GOA (10%) (figure 3(e)) and PEG-GOA (30%) (figure 3(f)) after cross-linking is noticeable. This observation demonstrates the effects of cross-linking on the surface morphology of GOA.

We investigated the morphology of PEG-GO flakes using TEM with EDS. The results are shown in figure 4, which contrasts with the flat sheet morphology of pure GO observed in our previous work [42]. By comparison, the formation of nano-scale wrinkles upon the cross-linking is observable on the PEG-GO flake as displayed in figure 4(a). In figures 4(d)–(f), the EDS analysis shows the existence of carbon, nitrogen, and oxygen on the PEG-GO flake. Notably, since nitrogen is not the elemental composition of pure GO, the significant distribution of nitrogen observed in figure 4(**e**) further supports the successful interaction between GO and PEGDA.

The water uptake (gg^{-1}) at different RH was calculated to measure the water adsorption behaviours of pure GOA and cross-linked PEG-GOA. Figure 5(a) clearly shows that when the PEGDA mass fraction was increased by 10%, the water uptake significantly

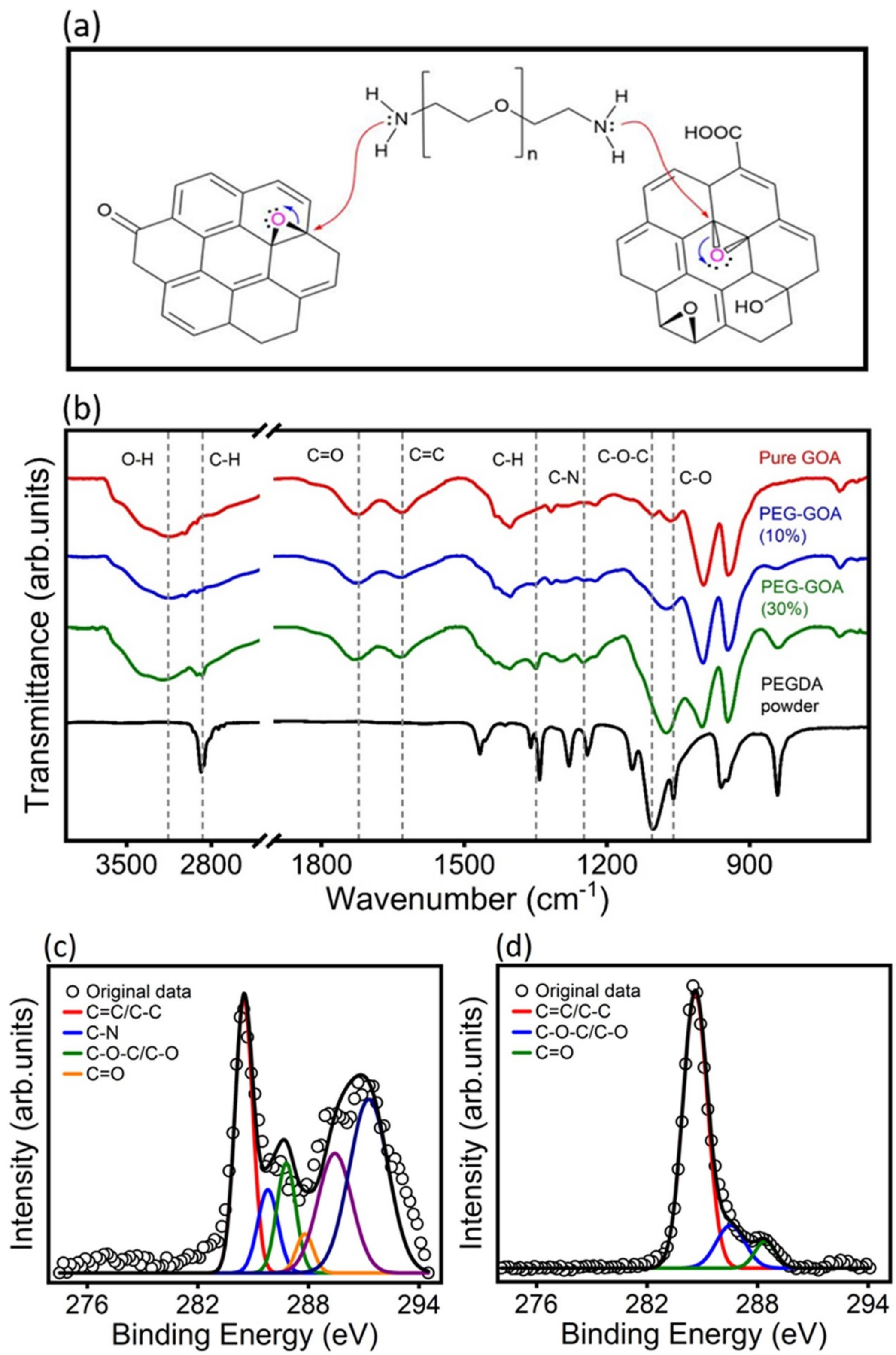

Figure 1. (a) Schematic graph of cross-linking between PEGDA and graphene oxide (epoxy groups are highlighted in purple). (b) Fourier transform infrared (FT-IR) spectrum of PEGDA powder, pure GOA, PEG-GOA (10%), and PEG-GOA (30%). C1s x-ray photoelectron spectroscopy (XPS) of (c) pure GOA, and (d) PEG-GOA.

increased from 0.362 gg^{-1} to 0.605 gg^{-1}. After exhibiting the highest water uptake of PEG-GOA, when the mass fraction of PEGDA exceeded 15%, the water uptake gradually declined, remaining at 0.435 gg^{-1} when the content reached 30%. This finding suggests that the higher addition of PEGDA may restrain the swelling of PEG-GOA, thereby limiting the water adsorption capacity in the interlayer space. This result is also supported by the obtained XRD patterns of PEG-GOA (10%) and PEG-GOA (30%) treated

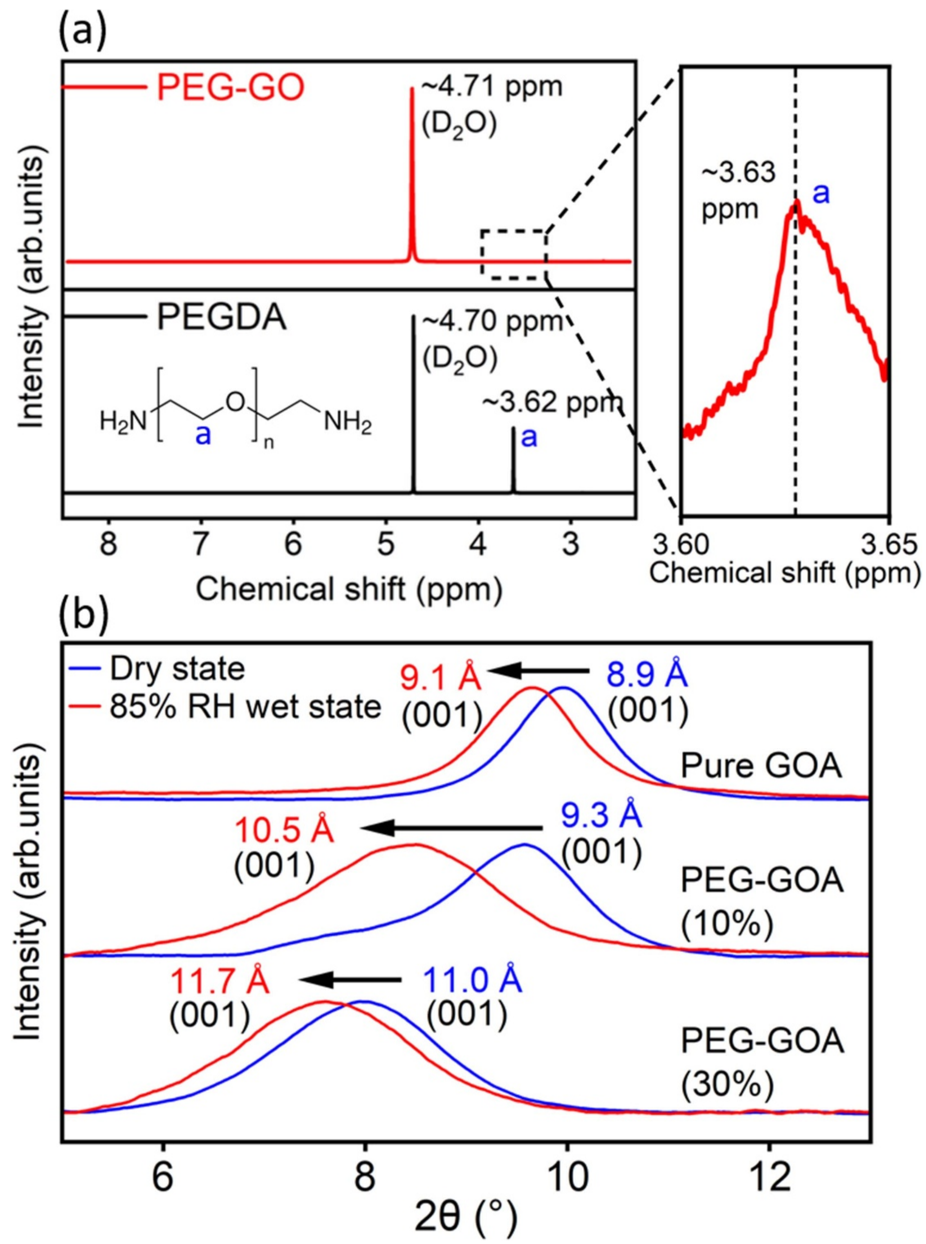

Figure 2. (a) Liquid-state ^{1}H nuclear magnetic resonance (NMR) spectra of PEGDA solution (black curve) in D_2O, and PEG-GO solution (red curve) in D_2O. (b) X-ray diffraction (XRD) patterns of the (001) peak of dried pure and cross-linked PEG-GOA samples and water adsorbed pure and cross-linked PEG-GOA samples at a relative humidity of 85%.

at the same RH as discussed above. As shown in figure 5(b), the adsorption capacities of pure GOA and PEG-GOA were determined by measuring the water uptake after 24 h at different partial pressures. After cross-linking, PEG-GOA (10%) and PEG-GOA (30%) exhibited consistently higher adsorption capacities than pure GOA. Particularly at a partial pressure of 2.69 kPa, PEG-GOA (10%) achieved a water uptake of 0.59 gg^{-1}, significantly higher than the 0.37 gg^{-1} of pure GOA, suggesting that the introduction of abundant alkoxy groups through cross-linking remarkably enhanced the adsorption capacity.

Figures 5(c)–(f) display the continuous water uptake within 5 h at different RH. Cross-linked PEG-GOA obtained consistently greater water uptake than that of pure GOA. In detail, at RH of 55%, PEG-GOA (10%) exhibited a water uptake ∼2 times that of pure GOA. Furthermore, at RH of 65%, 75%, and 85%, PEG-GOA (10%) all performed over 87% improvements in water uptake compared to pure GOA.

To further understand the interaction with water molecules after cross-linking, the desorption behaviours of moisture-adsorbed pure GOA and cross-linked PEG-GOA were tested at RH of 35% and 20%. As shown in figures 6(a) and (b), pure GOA required ∼80 min to desorb the captured water. In contrast, PEG-GOA (10%) and PEG-GOA (30%) exhibited continuous reductions of water uptake in the following 100 min. We performed 13 adsorption–desorption cycles to measure the stability

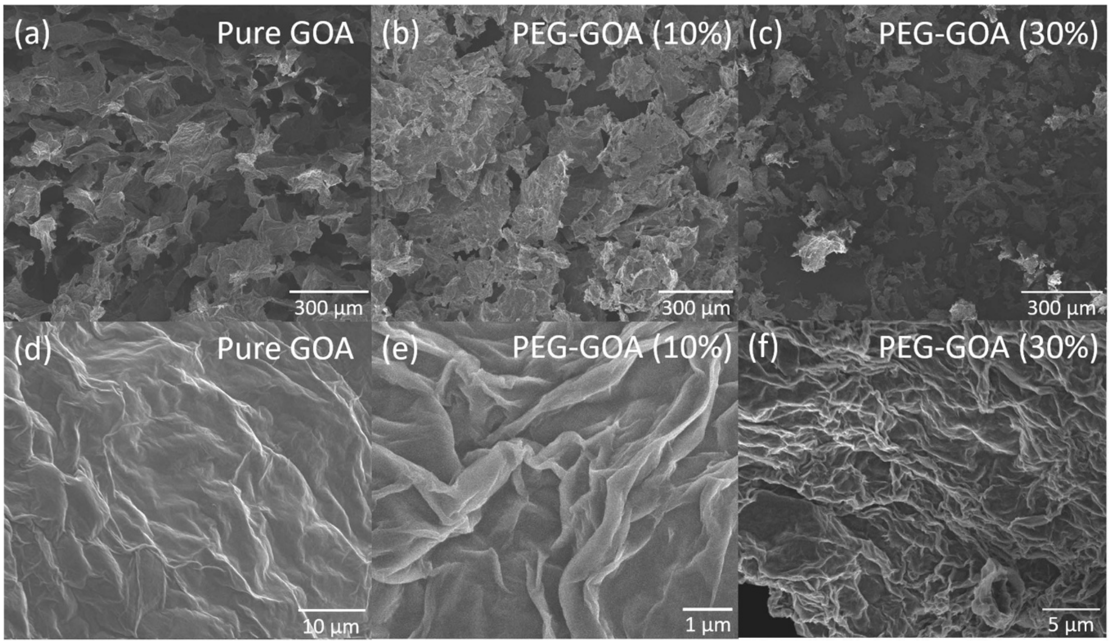

Figure 3. (a)–(f) Scanning electron microscope (SEM) images of pure GOA (a), (d), PEG-GOA (10%) (b), (e), and PEG-GOA (30%) (c), (f).

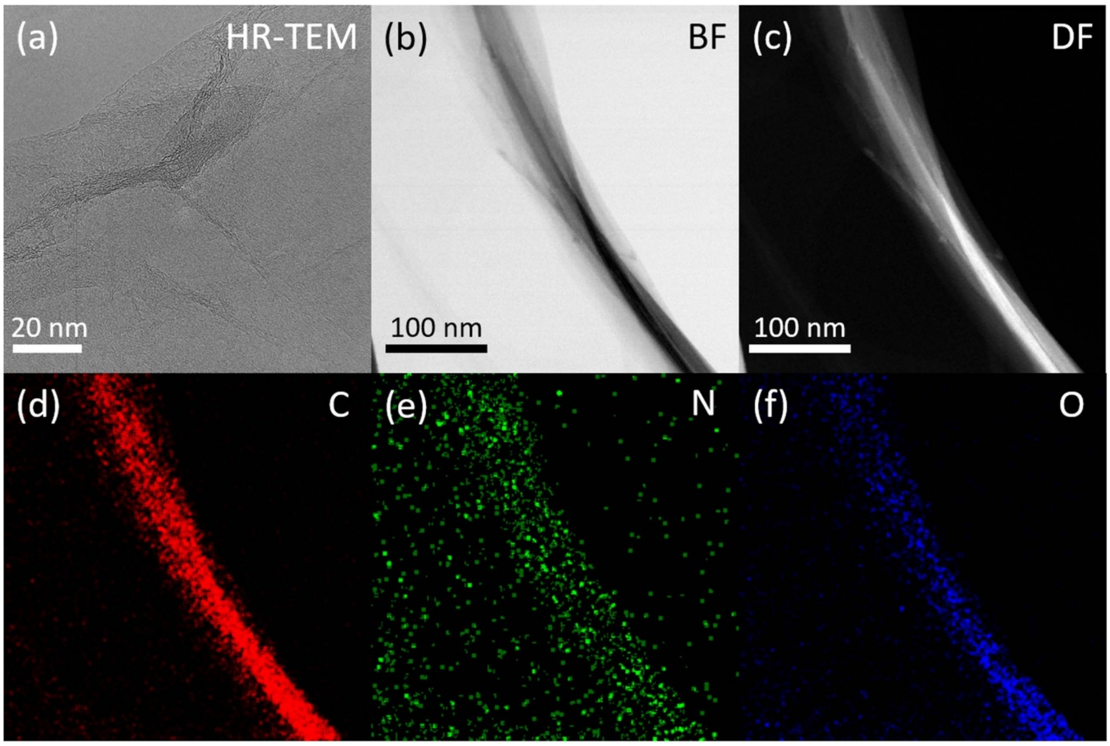

Figure 4. (a)–(c) High-resolution transmission electron microscope (HR-TEM) images of PEG-GO (a), bright-field (b), and dark-field images (c). (d)–(f) energy dispersive spectroscopy (EDS)-based elemental images of carbon (d), nitrogen (e), and oxygen (f).

of cross-linked PEG-GOA. In each cycle, pure GOA and PEG-GOA were first exposed to an RH of 85% to adsorb moisture for 24 h, followed by water desorption at a RH of 20% for 1 h. As shown in figure 6(c), after 13 cycles, the water uptake of pure GOA decreased by 0.13 gg^{-1}, while the water uptake of PEG-GOA (10%) and PEG-GOA (30%) showed slight decreases of 0.09 gg^{-1} and 0.06 gg^{-1}, respectively. Hence, the increased cross-linking effectively promotes the stability of PEG-GOA. As shown in figure 6(d), in desorption cycles, the mass of pure GOA decreased from 106.45–103.55 mg. In contrast,

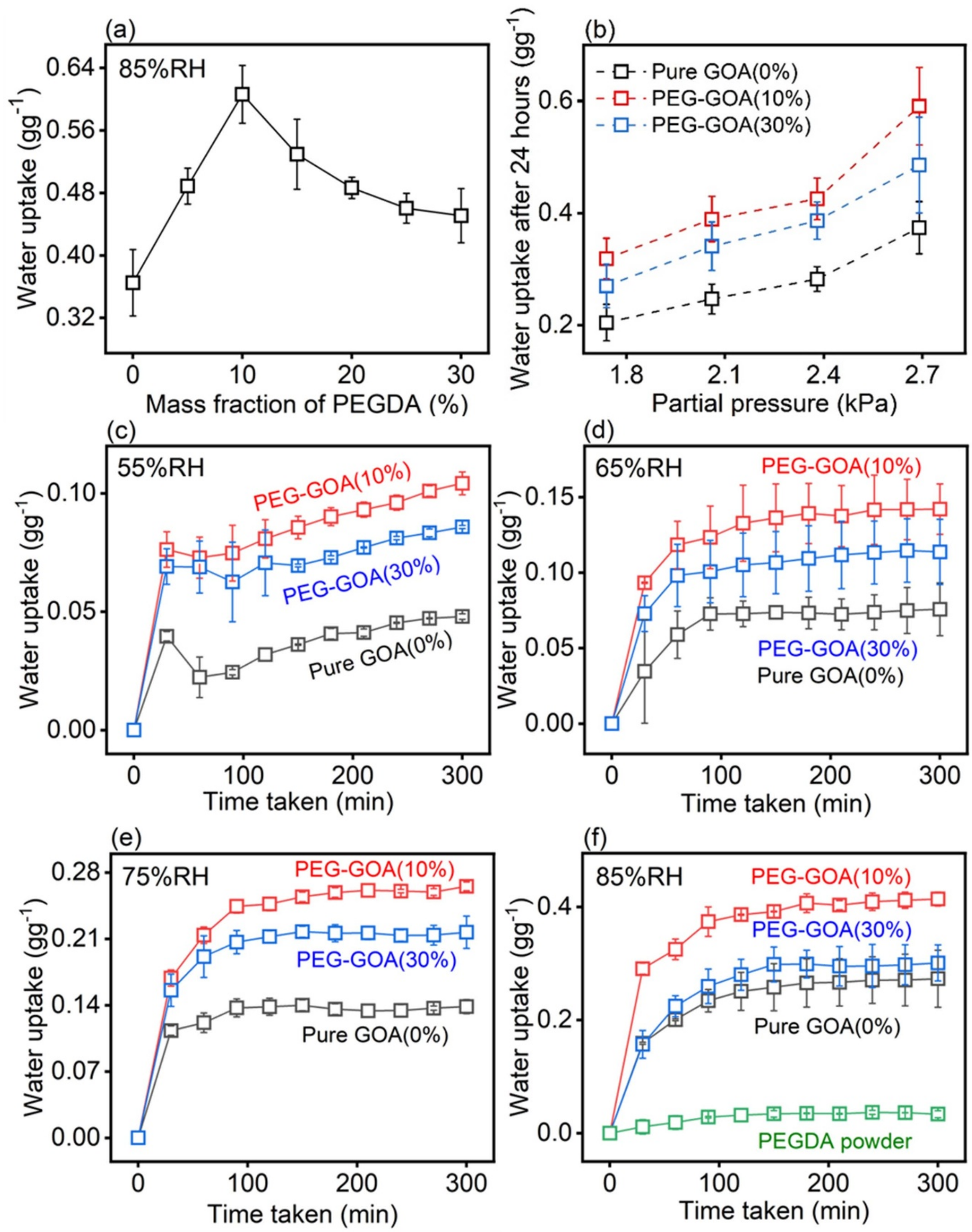

Figure 5. (a) Variations of water uptake of pure GOA and PEG-GOA after 24 h with improved mass fractions at a controlled RH of 85%. (b) Adsorption capacity of pure GOA and cross-linked PEG-GOA in different partial pressures. Adsorption measurements for pure GOA, PEG-GOA (10%), and PEG-GOA (30%) over five hours at RH of (c) 55%; (d) 65%; (e) 75%, and (f) 85%. Freeze-dried PEGDA powder marked in green curve in (f) shows low water uptake.

the mass reduction of PEG-GOA (10%) and PEG-GOA (30%) was 11.34 mg and 12.84 mg after 13 cycles. This suggests that the covalent cross-linking significantly improved the water retention over cycles. Furthermore, in figure 6(e), we conducted FTIR spectroscopy after the adsorption–desorption cycle to see the stability of the surface chemistry of PEG-GOA samples. The result shows that the surface chemistry of PEG-GOA (10%) and PEG-GOA (30%) remained unchanged after the adsorption–desorption cycle because the characteristic peaks corresponding to CH, CH_2, and C–N bonds are located highly consistent with the FTIR spectra of unused PEG-GOA (10%) and PEG-GOA (30%).

In bulk powder form, as shown in figure 5(f), PEGDA exhibits low water uptake at the RH of 85%. As schematically illustrated in figures 7(a)–(d), this can be attributed to the internal entanglement of polymer chains in bulk powder form. Hence, the interaction with the internal polymer chains is

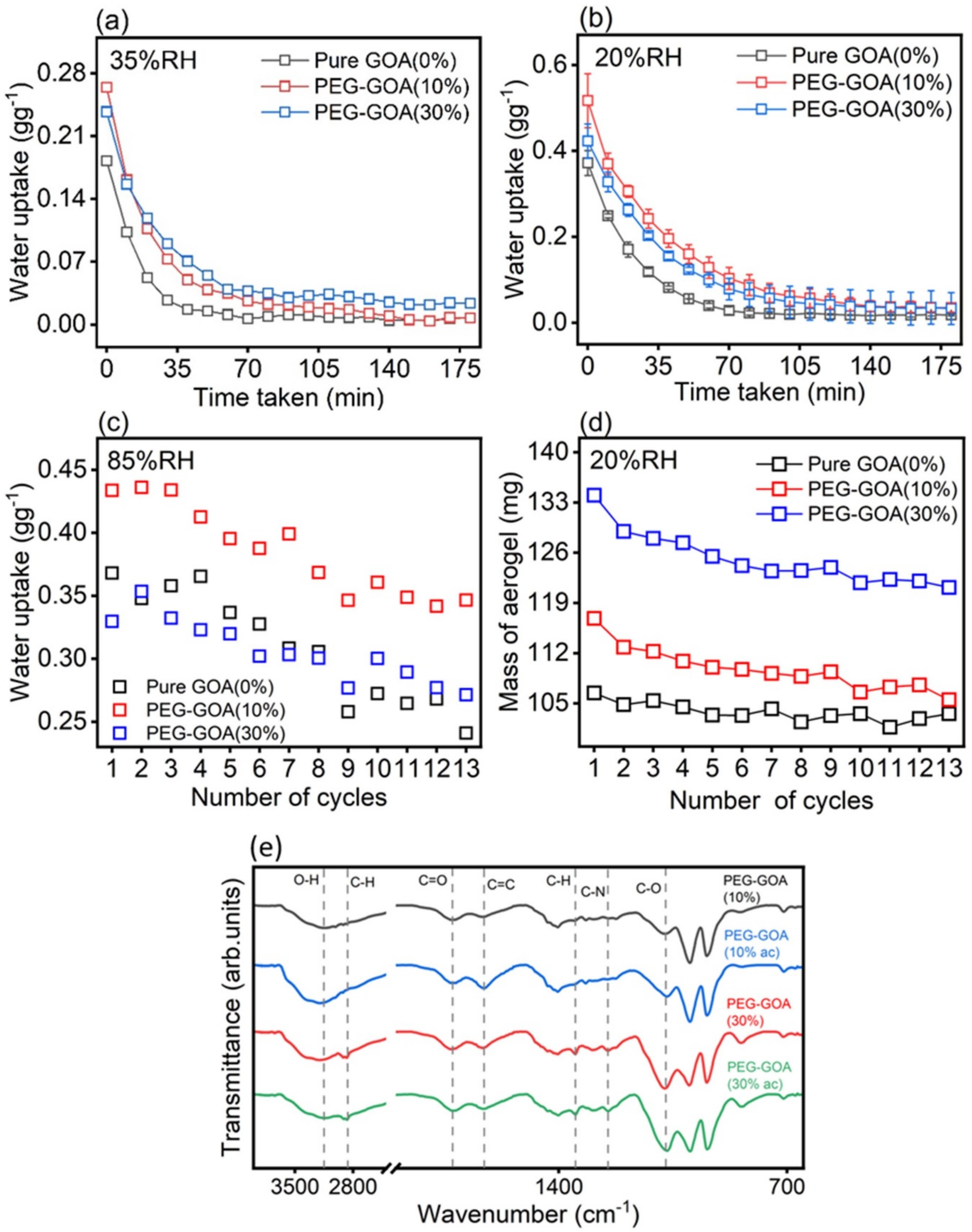

Figure 6. Desorption behaviours of pure GOA and PEG-GOA in RH of (a) 35% and (b) 20% within 180 min; (c) cycles adsorption tests of pure GOA and PEG-GOA at RH of 85% for 24 h; and (d) variations in the mass of aerogel samples in cycles desorption tests. (e) Fourier-transform infrared spectra of unused PEG-GOA (10%) (black curve), PEG-GOA (30%) (red curve), PEG-GOA (10% ac, blue curve) and PEG-GOA (30% ac, green-curve), ac for after adsorption–desorption cycle.

limited, making the water molecules primarily attach to the surface of PEGDA powder. Upon the covalent cross-linking with GO, the abundant alkoxy groups on dispersed PEGDA are exposed to water molecules due to the swelling-induced stretching of chains. Therefore, the greater number of exposed hydrophilic functional groups and the swollen interlayer space caused by this synergistic effect significantly facilitated the water uptake in PEG-GOA (10%). However, excessive PEGDA chains lead to the accumulation of polymers in the interlayer space of GO, limiting the moisture interaction with the polymer chains. Despite this, the dispersed PEGDA in the GOA framework still has a greater specific surface area than the bulk PEGDA powder, making PEG-GOA (30%) exhibit enhanced water uptake, while is relatively lower than that of PEG-GOA (10%).

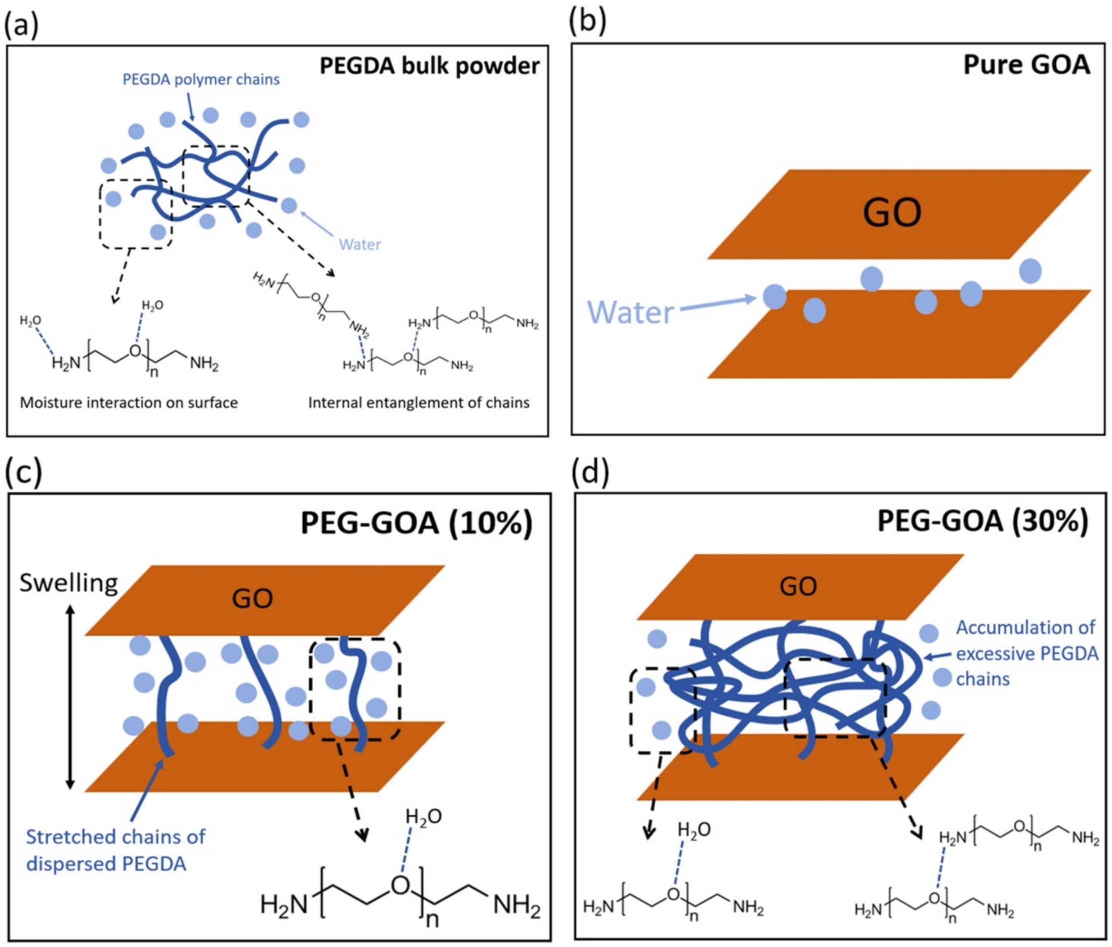

Figure 7. Schematic graphs of the mechanism hypothesis of moisture adsorption of (a) bulk PEGDA powder, (b) pure GOA, (c) cross-linked PEG-GOA (10%), and (d) cross-linked PEG-GOA (30%).

4. Conclusion

In summary, this work highlights the potential of hygroscopic covalent cross-linking in GO-based moisture adsorption and further discusses the role of PEG-based cross-linking in moisture interaction. Covalently cross-linked PEG-GOA effectively improves moisture adsorption behaviours. Compared to pure GOA, introducing abundant hydrophilic alkoxy groups from PEGDA improves the water uptake of PEG-GOA at different RH. Moreover, the covalent cross-linked PEG polymers not only lead to a stronger interaction with water molecules but also develop the stability and water retention of PEG-GOA. Based on the discussed synergistic effect behind PEG-GO, we believe that the covalent cross-linking strategies may provide insights for future design in GO-based atmospheric water capture applications.

Data availability statement

All data that support the findings of this study are included within the article (and any supplementary files).

Acknowledgments

This research was supported by the Australian Research Council through the Centre of Excellence for Carbon Science and Innovation (CE230100032). X R and T L acknowledge the UNSW UIPA Scholarship.

Conflict of interest

There are no conflicts to declare.

Author contributions

Zhijian Cao 0009-0006-4055-1677
Conceptualization (lead), Investigation (lead), Methodology (lead), Writing – original draft (equal)

Xiaojun Ren
Conceptualization (supporting), Investigation (supporting), Methodology (supporting), Writing – review & editing (supporting)

Tongxi Lin 0009-0004-3406-9011
Conceptualization (supporting), Formal analysis (supporting), Investigation (supporting), Methodology (supporting), Writing – original draft (supporting), Writing – review & editing (supporting)

Yuta Nishina 0000-0002-4958-1753
Formal analysis (supporting), Investigation (supporting), Methodology (supporting), Writing – review & editing (supporting)

Masamichi Yoshimura
Investigation (supporting), Methodology (supporting)

Rakesh Joshi 0000-0002-7497-9499
Conceptualization (lead), Formal analysis (supporting), Investigation (supporting), Methodology (supporting), Project administration (lead), Supervision (lead), Writing – review & editing (supporting)

References

[1] Hunger B, Matysik S, Heuchel M, Geidel E and Toufar H 1997 Adsorption of water on zeolites of different types *J. Therm. Anal.* **49** 553–65
[2] Simonova I A, Freni A, Restuccia G and Aristov Y I 2009 Water sorption on composite "silica modified by calcium nitrate" *Microporous Mesoporous Mater.* **122** 223–8
[3] Kim H, Yang S, Rao S R, Narayanan S, Kapustin E A, Furukawa H, Umans A S, Yaghi O M and Wang E N 2017 Water harvesting from air with metal-organic frameworks powered by natural sunlight *Science* **356** 430–4
[4] Furukawa H, Gándara F, Zhang Y-B, Jiang J, Queen W L, Hudson M R and Yaghi O M 2014 Water adsorption in porous metal–organic frameworks and related materials *J. Am. Chem. Soc.* **136** 4369–81
[5] Qi H *et al* 2019 An interfacial solar-driven atmospheric water generator based on a liquid sorbent with simultaneous adsorption–desorption *Adv. Mater.* **31** 1903378
[6] Wei N, Peng X and Xu Z 2014 Understanding water permeation in graphene oxide membranes *ACS Appl. Mater. Interfaces* **6** 5877–83
[7] Wen X, Foller T, Jin X, Musso T, Kumar P and Joshi R 2022 Understanding water transport through graphene-based nanochannels via experimental control of slip length *Nat. Commun.* **13** 5690
[8] Foller T *et al* 2022 Mass transport via in-plane nanopores in graphene oxide membranes *Nano Lett.* **22** 4941–8
[9] Liu L, Zhang R, Liu Y, Tan W and Zhu G 2018 Insight into hydrogen bonds and characterization of interlayer spacing of hydrated graphene oxide *J. Mol. Model.* **24** 137
[10] Chen B, Jiang H, Liu X and Hu X 2017 Observation and analysis of water transport through graphene oxide interlamination *J. Phys. Chem. C* **121** 1321–8
[11] Sun P, Zhu M, Wang K, Zhong M, Wei J, Wu D, Xu Z and Zhu H 2013 Selective ion penetration of graphene oxide membranes *ACS Nano* **7** 428–37
[12] Foller T and Joshi R 2024 Let's discuss: when can we call a thin film 2-dimensional? *Curr. Opin. Solid State Mater. Sci.* **32** 101186
[13] Joshi M, Ren X, Lin T and Joshi R 2025 Mechanistic insights into gas adsorption on 2D materials *Small* **21** 2406706
[14] Karton A, Foller T and Joshi R 2024 Catalyzing epoxy oxygen migration on the basal surface of graphene oxide using strong hydrogen-bond donors *Chem. Commun.* **60** 7049–52
[15] Lin T, Wen X, Ren X, Quintano V, Andreeva D V, Novoselov K S and Joshi R 2025 Recent advances in graphene-based membranes with nanochannels and nanopores *Small Struct.* **6** 2400320
[16] Deng J, You Y, Bustamante H, Sahajwalla V and Joshi R K 2017 Mechanism of water transport in graphene oxide laminates *Chem. Sci.* **8** 1701–4
[17] Cao Z, Wen X, Quintano V and Joshi R 2023 On the role of functionalization in graphene-moisture interaction *Curr. Opin. Solid State Mater. Sci.* **27** 101122
[18] Dreyer D R, Park S, Bielawski C W and Ruoff R S 2010 The chemistry of graphene oxide *Chem. Soc. Rev.* **39** 228–40
[19] Chen D, Feng H and Li J 2012 Graphene oxide: preparation, functionalization, and electrochemical applications *Chem. Rev.* **112** 6027–53
[20] Huang X, Qi X, Boey F and Zhang H 2012 Graphene-based composites *Chem. Soc. Rev.* **41** 666–86
[21] Loh K P, Bao Q, Ang P K and Yang J 2010 The chemistry of grapheme *J. Mater. Chem.* **20** 2277–89
[22] Lerf A, Buchsteiner A, Pieper J, Schöttl S, Dekany I, Szabo T and Boehm H P 2006 Hydration behavior and dynamics of water molecules in graphite oxide *J. Phys. Chem. Solids* **67** 1106–10
[23] Wei N, Peng X and Xu Z 2014 Breakdown of fast water transport in graphene oxides *Phys. Rev. E* **89** 012113
[24] Nair R R, Wu H A, Jayaram P N, Grigorieva I V and Geim A K 2012 Unimpeded permeation of water through helium-leak-tight graphene-based membranes *Science* **335** 442–4
[25] Zhu Y, Murali S, Cai W, Li X, Suk J W, Potts J R and Ruoff R S 2010 Graphene and graphene oxide: synthesis, properties, and applications *Adv. Mater.* **22** 3906–24
[26] Lian B, De Luca S, You Y, Alwarappan S, Yoshimura M, Sahajwalla V, Smith S C, Leslie G and Joshi R K 2018 Extraordinary water adsorption characteristics of graphene oxide *Chem. Sci.* **9** 5106–11
[27] Carr A J, Lee S E and Uysal A 2023 Ion and water adsorption to graphene and graphene oxide surfaces *Nanoscale* **15** 14319–37
[28] Wang X, Yang D, Zhang M, Hu Q, Gao K, Zhou J and Yu Z-Z 2022 Super-hygroscopic calcium chloride/graphene oxide/poly(N-isopropylacrylamide) gels for spontaneous harvesting of atmospheric water and solar-driven water release *ACS Appl. Mater. Interfaces* **14** 33881–91
[29] Anjali C, Muhammed Razi P, Thayyil MS and Neeroli Kizhakayil R 2024 Desiccant-embedded graphene oxide/PVA Gels for atmospheric water harvesting *ACS Appl. Nano Mater.* **7** 18535–44
[30] Ghosh S and Chatterjee K 2020 Poly(ethylene glycol) functionalized graphene oxide in tissue engineering: a review on recent advances *Int. J. Nanomed.* **15** 5991–6006
[31] Shen J, Shi M, Yan B, Ma H, Li N, Hu Y and Ye M 2010 Covalent attaching protein to graphene oxide via diimide-activated amidation *Colloids Surf. B* **81** 434–8
[32] Parsamehr P S, Zahed M, Tofighy M A, Mohammadi T and Rezakazemi M 2019 Preparation of novel cross-linked graphene oxide membrane for desalination applications using (EDC and NHS)-activated graphene oxide and PEI *Desalination* **468** 114079
[33] Bansal S A, Singh S, Srivastava A, Singh A P and Kumar S 2021 Covalent attachment of 2D graphene oxide (GO) sheets with poly allylamine (PAA) for enhanced mechanical performance: theoretical and experimental study *Polymer* **213** 123195
[34] Vacchi I A, Spinato C, Raya J, Bianco A and Ménard-Moyon C 2016 Chemical reactivity of graphene oxide towards amines elucidated by solid-state NMR *Nanoscale* **8** 13714–21
[35] Islam F *et al* 2023 PEGylated graphene oxide as a nanodrug delivery vehicle for podophyllotoxin

(GO/PEG/PTOX) and *in vitro* α-amylase/α-glucosidase inhibition activities *ACS Omega* **8** 20550–60
[36] Bai J, Liu Y and Jiang X 2014 Multifunctional PEG-GO/CuS nanocomposites for near-infrared chemo-photothermal therapy *Biomaterials* **35** 5805–13
[37] Kazempour M, Namazi H, Akbarzadeh A and Kabiri R 2019 Synthesis and characterization of PEG-functionalized graphene oxide as an effective pH-sensitive drug carrier *Artif. Cells Nanomed. Biotechnol.* **47** 90–94
[38] Xu Z, Zhu S, Wang M, Li Y, Shi P and Huang X 2015 Delivery of paclitaxel using PEGylated graphene oxide as a nanocarrier *ACS Appl. Mater. Interfaces* **7** 1355–63
[39] Zhao D, Zhao J, Ji Y, Liu G, Liu S and Jin W 2018 Facilitated water-selective permeation via PEGylation of graphene oxide membrane *J. Membr. Sci.* **567** 311–20
[40] Ren X *et al* 2025 Synergetic hydrogen-bond network of functionalized graphene and cations for enhanced atmospheric water capture *Proc. Natl Acad. Sci.* **122** e2508208122
[41] Rakesh J, Xiao S, Tobias F, Dali J, Xiaojun R and Llewellyn O 2025 A Graphene Oxide Aerogel U.S. Patent Application No. 18/689,275
[42] Chen H, Lin T, Ramadhan Z R, Rawal A, Nishina Y, Karton A, Ren X and Joshi R 2025 Organic solvent transport through reduced graphene oxide membranes with controlled oxygen content *Carbon* **243** 120539
[43] Lin T, Wu Y, Chen H, Ren X and Joshi R 2025 Graphene oxide-polyvinyl alcohol nanofiltration membranes for efficient dye removal in practical conditions *J. Membr. Sci.* **719** 123736
[44] Wang F *et al* 2024 Structure-dependent lithium storage characteristics of Fe_3O_4/rGO aerogels *Carbon* **222** 119003
[45] Bi H, Yin K, Xie X, Ji J, Wan S, Sun L, Terrones M and Dresselhaus M S 2013 Ultrahigh humidity sensitivity of graphene oxide *Sci. Rep.* **3** 2714
[46] Paterakis G *et al* 2022 Highly sensitive and ultra-responsive humidity sensors based on graphene oxide active layers and high surface area laser-induced graphene electrodes *Nanomaterials* **12** 2684
[47] Surekha G, Krishnaiah K V, Ravi N and Padma Suvarna R 2020 FTIR, Raman and XRD analysis of graphene oxide films prepared by modified Hummers method *J. Phys.: Conf. Ser.* **1495** 012012
[48] Chen M, Zhang C, Li X, Zhang L, Ma Y, Zhang L, Xu X, Xia F, Wang W and Gao J 2013 A one-step method for reduction and self-assembling of graphene oxide into reduced graphene oxide aerogels *J. Mater. Chem. A* **1** 2869
[49] Si W, Wu X, Zhou J, Guo F, Zhuo S, Cui H and Xing W 2013 Reduced graphene oxide aerogel with high-rate supercapacitive performance in aqueous electrolytes *Nanoscale Res. Lett.* **8** 247
[50] Georgieva M, Gospodinova Z, Keremidarska-Markova M, Kamenska T, Gencheva G and Krasteva N 2021 PEGylated nanographene oxide in combination with near-infrared laser irradiation as a smart nanocarrier in colon cancer targeted therapy *Pharmaceutics* **13** 424
[51] Charmi J, Nosrati H, Mostafavi Amjad J, Mohammadkhani R and Danafar H 2019 Polyethylene glycol (PEG) decorated graphene oxide nanosheets for controlled release curcumin delivery *Heliyon* **5** e01466
[52] Xu J, Xing W, Zhao L, Guo F, Wu X, Xu W and Yan Z 2015 The CO_2 storage capacity of the intercalated diaminoalkane graphene oxides: a combination of experimental and simulation studies *Nanoscale Res. Lett.* **10** 318
[53] Borges-Vilches J, Poblete J, Gajardo F, Aguayo C and Fernández K 2021 Graphene oxide/polyethylene glycol aerogel reinforced with grape seed extracts as wound dressing *J. Mater. Sci.* **56** 16082–96
[54] Scaffaro R, Maio A, Lopresti F, Giallombardo D, Botta L, Bondì M L and Agnello S 2016 Synthesis and self-assembly of a PEGylated-graphene aerogel *Compos. Sci. Technol.* **128** 193–200
[55] Chen C, Zhu X and Chen B 2018 Covalently cross-linked graphene oxide aerogel with stable structure for high-efficiency water purification *Chem. Eng. J.* **354** 896–904
[56] Kang W, Cui Y, Yang Y, Zhao Z, Wang X and Liu X 2021 An acid induction strategy to construct an ultralight and durable amino-functionalized graphene oxide aerogel for enhanced quinoline pollutants extraction from coking wastewater *Chem. Eng. J.* **412** 128686
[57] Jin T, Easton C D, Tang Y, Yin H and Hao X 2018 Nitrogen-doped graphene oxide monoliths crosslinked by short chain aliphatic amines *J. Hazard. Mater.* **357** 100–8
[58] Chen X, Wang X and Fang D 2020 A review on C1s XPS-spectra for some kinds of carbon materials *Fuller. Nanotub. Carbon Nanostruct.* **28** 1048–58
[59] Lin W-C, Lo W-C, Li J-X, Wang Y-K, Tang J-F and Fong Z-Y 2021 *In situ* XPS investigation of the x-ray-triggered decomposition of perovskites in ultrahigh vacuum condition *npj Mater. Degrad.* **5** 13
[60] Garriga R *et al* 2017 Multifunctional, biocompatible and pH-responsive carbon nanotube- and graphene oxide/tectomer hybrid composites and coatings *Nanoscale* **9** 7791–804
[61] Zhang X, Sui Z, Xu B, Yue S, Luo Y, Zhan W and Liu B 2011 Mechanically strong and highly conductive graphene aerogel and its use as electrodes for electrochemical power sources *J. Mater. Chem.* **21** 6494
[62] Liu Y, Jiang H, Liu C, Ge Y, Wang L, Zhang B, He H and Liu S 2019 Influence of functional groups on toxicity of carbon nanomaterials *Atmos. Chem. Phys.* **19** 8175–87
[63] Acocella M R, Corcione C E, Giuri A, Maggio M, Maffezzoli A and Guerra G 2016 Graphene oxide as a catalyst for ring opening reactions in amine crosslinking of epoxy resins *RSC Adv.* **6** 23858–65
[64] Zhang B, Zhang H, Myers B K, Elupula R, Jayawickramarajah J and Grayson S M 2014 Determination of polyethylene glycol end group functionalities by combination of selective reactions and characterization by matrix assisted laser desorption/ionization time-of-flight mass spectrometry *Anal. Chim. Acta* **816** 28–40
[65] Hao J, Gao Y, Zheng C, Liu J, Hu J and Ju Y 2018 Natural-product-tailored polyurethane: size-dictated construction of polypseudorotaxanes with cyclodextrin–triterpenoid pairs *ACS Macro Lett.* **7** 1131–7
[66] Liu Q, Gupta K M, Xu Q, Liu G and Jin W 2019 Gas permeation through double-layer graphene oxide membranes: the role of interlayer distance and pore offset *Sep. Purif. Technol.* **209** 419–25
[67] Zheng S, Tu Q, Urban J J, Li S and Mi B 2017 Swelling of graphene oxide membranes in aqueous solution: characterization of interlayer spacing and insight into water transport mechanisms *ACS Nano* **11** 6440–50